

Correlation effects in the iron pnictides

Qimiao Si¹, Elihu Abrahams², Jianhui Dai³, Jian-Xin Zhu⁴

¹ Department of Physics and Astronomy, Rice University, Houston, Texas 77005, USA

² Center for Materials Theory, Department of Physics and Astronomy, Rutgers University, Piscataway, New Jersey 08855, USA

³ Zhejiang Institute of Modern Physics, Zhejiang University, Hangzhou 310027, China

⁴ Theoretical Division, Los Alamos National Laboratory, Los Alamos, New Mexico 87545, USA

Abstract. One of the central questions about the iron pnictides concerns the extent to which their electrons are strongly correlated. Here we address this issue through the phenomenology of the charge transport and dynamics, single-electron excitation spectrum, and magnetic ordering and dynamics. We outline the evidence that the parent compounds, while metallic, have electron interactions that are sufficiently strong to produce *incipient* Mott physics. In other words, in terms of the strength of electron correlations compared to the kinetic energy, the iron pnictides are closer to intermediately-coupled systems lying at the boundary between itinerancy and localization, such as V_2O_3 or Se-doped NiS_2 , rather than to simple antiferromagnetic metals like Cr. This level of electronic correlations produces a new small parameter for controlled theoretical analyses, namely the fraction of the single-electron spectral weight that lies in the coherent part of the excitation spectrum. Using this expansion parameter, we construct the effective low-energy Hamiltonian and discuss its implications for the magnetic order and magnetic quantum criticality. Finally, this approach sharpens the notion of magnetic frustration for such a metallic system, and brings about a multiband matrix t - J_1 - J_2 model for the carrier-doped iron pnictides.

1. Introduction

Two decades after the discovery of the cuprate superconductors, we finally have a new and copper-free family of materials with high temperature superconductivity [1, 2]. Naturally, these iron pnictides have generated an enormous interest, both theoretical and experimental. One of the intriguing features of the iron pnictides is the phase diagram itself. Typically, superconductivity arises from carrier doping of the parent iron arsenides that are metallic antiferromagnets.

A central question is how strongly correlated are the iron pnictides? It is meaningful to address the issue in the normal state, given that the energy scales for the normal state electronic and magnetic excitations appear to be considerably larger than those for superconductivity. Moreover, it is adequate to focus on the $3d$ electrons of the Fe atoms, which represent the majority of the electronic states near the Fermi energy. There is an important simplicity here, namely the Fe atoms, whose $3d$ orbitals dominate the states near the Fermi energy, are arranged into square-lattice layers. But there is also complication: several if not all of the five $3d$ orbitals need to be taken into account [3, 4, 5, 6, 7, 8, 9].

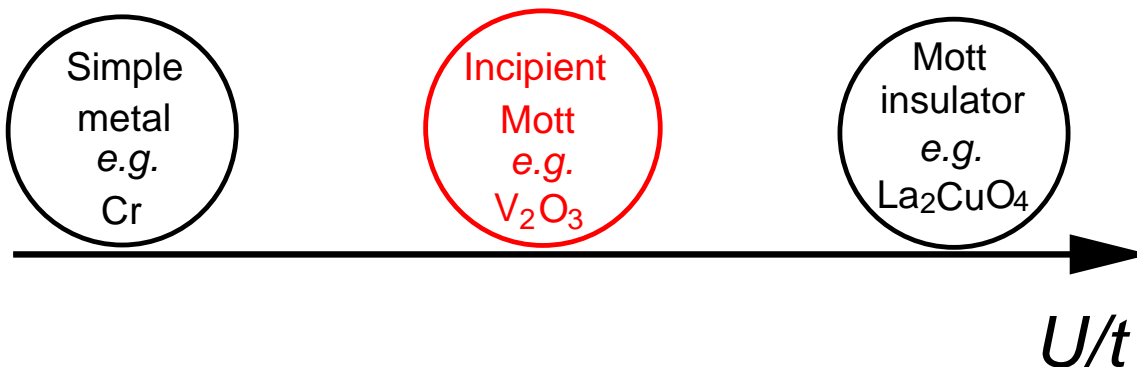


Figure 1. Different reference regimes corresponding to different ranges of interaction strength. When the interaction is large compared to the Fermi energy, the system is in a Mott-insulating state. In the opposite limit, it is a simple metal; Cr is a canonical example for this regime. For intermediate values of interaction close to but below the Mott transition threshold, the system is metallic but has a sizable fraction of single-electron spectral weight in an incoherent part as a precursor to the Mott localization; V_2O_3 and $NiS_{2-x}Se_x$ are known systems belonging to this regime.

Consider the parent iron pnictides, which may be described in terms of six electrons occupying the nearly degenerate $3d$ orbitals at each site of the square lattice. We can frame the discussion about the strength of electron correlations in terms of Fig. 1, which divides partially filled lattice electron systems with integer number of electrons into three broad categories:

- * When the interactions are strong compared to the kinetic energy or bandwidth (large U/t in Fig. 1), the system would in general be a Mott insulator. This would be a multi-orbital analog of what happens in the undoped cuprates, and it clearly

does not apply here since the parent iron arsenides are metallic.

- * When the interactions are relatively weak compared to the kinetic energy, we have a simple metal. This would be the analog of Cr [10, 11].
- * When the interactions are comparable to the kinetic energy, the system is metallic but is on the verge of localization. Typical examples of such incipient Mott systems are V_2O_3 and Se-doped NiS_2 [12].

In the following, we extend our previous considerations [13, 14] and provide the phenomenological arguments that the iron pnictides are very different from the weakly-correlated cases like Cr, but are much more similar to the incipient Mott systems such as V_2O_3 and Se-doped NiS_2 . We then discuss how this placement of the iron pnictides at the boundary between itinerancy and localization serves as the basis to construct the low-energy effective Hamiltonian. The latter, in turn, allows a controlled analysis of the magnetic order and magnetic fluctuations in the iron pnictides.

2. Simple metals vs. metals proximate to Mott localization

There are several distinct aspects of physics in the different regimes discussed above. The degree of itinerancy and incipient localization is by definition different (see below). Relatedly, each regime has its own natural small parameter for controlled theoretical approaches. Finally, the difference in the small parameter in turn leads to different ways of treating the magnetism.

When the interaction is weak compared to the bandwidth (or Fermi energy), it is standard to use the non-interacting limit as the reference point, and adopt the interaction normalized by the kinetic energy as a small parameter for perturbation theory. In spite of the weak interaction, antiferromagnetism can still develop when the degree of Fermi-surface nesting is sufficiently large. Cr is the canonical example for this.

When interaction is of the order of the Fermi energy, the interaction normalized by the kinetic energy is no longer a small quantity. In order to treat the effect of interactions in a controlled fashion, we need to use a different reference point. One possibility is the point of the Mott transition, where the coherent electronic excitations have vanished and all the electronic excitations are incoherent. If we denote by w the fraction of the single-electron spectral weight that lies in the coherent part, w then serves as an emergent expansion parameter of the theory. This quantity provides a precise definition of the degree of itinerancy introduced earlier: a larger w means a larger degree of itinerancy and, by extension, a smaller degree of incipient localization.

In this approach, the reference point, at $w = 0$, already captures the magnetism associated with the localized moments. When w is non-zero, a perturbative treatment in w will lead to an effective low energy theory that couples the local moments to the itinerant coherent electronic excitations. Following our earlier work [13, 14], we will give the details of this construction in Sec. 5.

Physically, the incoherent excitations are non-perturbative effects that go beyond the Fermi liquid theory. They represent a precursor to the lower and upper Hubbard

bands in a Mott insulator, which itself is a phenomenon non-perturbative in interactions. As we shall see, the existence of these incoherent single-electron excitations will also have important consequences for the description of magnetic order and magnetic dynamics.

Our placement of the iron pnictides at the boundary of itinerancy and localization is guided by phenomenology. Related intermediate-coupling studies have also appeared in the literature [5, 15, 16, 17, 18, 19, 20, 21, 22, 23].

Systems known [25, 26, 27] to be in this category are V_2O_3 and $NiS_{2-x}Se_x$, whose phase diagram is shown schematically in Fig. 2. At room temperature and ambient pressure, V_2O_3 lies inside the paramagnetic metal part of its phase diagram and displays all the features of a “bad metal” (see below). Through the application of a negative chemical pressure (Cr doping for V), it can be explicitly tuned through a localization transition into a Mott insulator state. Similarly, $NiS_{2-x}Se_x$ can be tuned across the Mott transition as a function of the Se-doping for S. The transition has been extensively studied in terms of the dynamical mean field theory (DMFT) [28].

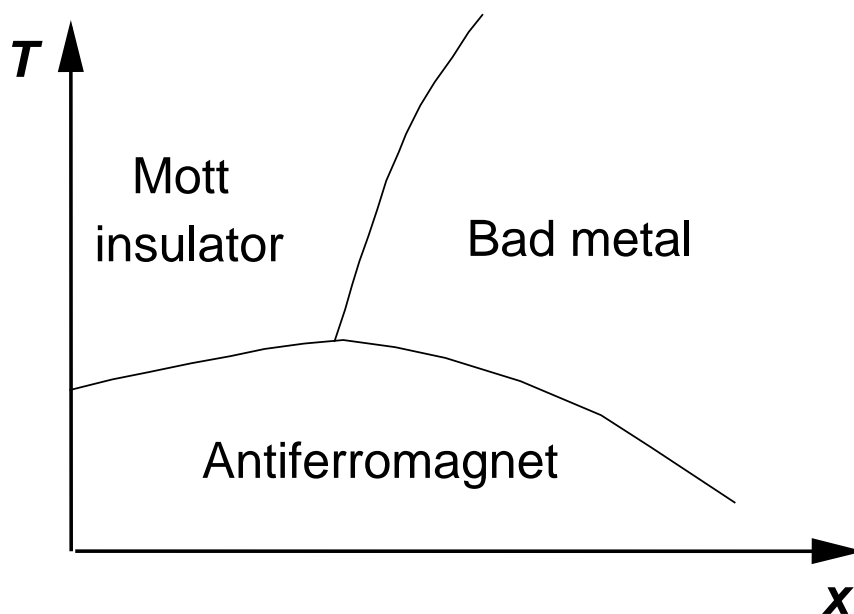


Figure 2. Schematic phase diagram of V_2O_3 and NiS_2 . x could be external pressure or chemical doping (Cr or Ti doping for V; Se doping for S). The bad-metal regime is referred to in Fig. 1 as the incipient-Mott regime. The antiferromagnetic region may be further divided into insulating and metallic phases.

3. Charge transport and dynamics

A metal near a Mott transition will be a bad metal, which can be operationally defined in terms of a large electrical resistivity at room temperature. The large resistivity corresponds to an effective mean free path ℓ that is on the order of the average inter-electron spacing. It originates from the presence of incoherent electronic excitations, which represent the precursor to Mott localization. Note that our discussion of bad

metal shares some similarity with that of Ref. [29], although the issue of resistivity saturation at high temperatures does not come into play in our consideration.

Experiments on the charge transport and charge dynamics indeed show that the iron pnictides are bad metals. Consider first the electrical resistivity at room temperature; it is on the order of $5 \text{ m}\Omega \cdot \text{cm}$ for polycrystals [1] and $0.5 \text{ m}\Omega \cdot \text{cm}$ for single crystals [30, 31]. These yield a $k_F \ell$ of order unity.

Consider next the optical conductivity. The bad metal aspect is most clearly seen in the reduced Drude weight. Indeed, the Drude peak is hardly visible in polycrystal compounds [24, 32]. In single crystals, the Drude weight is relatively small [33, 34], and the fitted plasma frequency is of the order of that extracted for either V_2O_3 or doped cuprates.

The bad metal physics is also manifested in the higher-energy part of the optical spectra. Since the development of the incoherent excitations comes at the expense of the coherent excitations (and vice versa), spectral weight in the optical conductivity can redistribute between the relatively high energy range and the lowest energies. Indeed, a relatively small change of temperature has been shown [33, 34, 32] to induce a significant transfer of spectral weight between the low-frequency Drude part and the part at high energies (0.6-1.5 eV).

All these features have strong similarities to what have been observed in both V_2O_3 and $\text{NiS}_{2-x}\text{Se}_x$. At room temperature and ambient pressure, V_2O_3 lies inside the paramagnetic metal part of its phase diagram (*cf.* Fig. 2), and its electrical resistivity is of the order of $0.5 \text{ m}\Omega \cdot \text{cm}$ [25]. In contrast, Cr is a good metal, with a room-temperature resistivity that is very small, about $0.01 \text{ m}\Omega \cdot \text{cm}$ [35]. When converted into a mean free path, the value for V_2O_3 is compatible to inter-particle spacing while that for Cr is close to 100 times that of the inter-particle spacing.

Likewise, in V_2O_3 , the Drude weight is a relatively small part of the total spectral weight and the fitted plasma frequency is about 1.3 eV [36]. As expected, the Drude peak is eliminated when V_2O_3 is tuned into the Mott insulating state [37]. Finally, the temperature-induced transfer of spectral weight [38, 39] between the Drude part and the higher-energy ($\sim 0.5\text{--}1.5$ eV) part is well-established. Similar evolution of the optical conductivity has also been observed [40] in $\text{NiS}_{2-x}\text{Se}_x$, across its Mott transition.

4. Single-electron excitations

4.1. Coherent and incoherent excitations

At the single-particle level, the coherent and incoherent excitations will appear as a natural decomposition of the total density of states. Photoemission measurements in principle provide a measurement of the density of states, but the results for the iron pnictides are at this point still uncertain.

A recent angular-resolved photoemission (ARPES) measurement on BaFe_2As_2 [41] has indicated incoherent excitations at very high energies (around 7 eV). There are

satellite features at about 2-3 eV range as well, and whether they are entirely due to the interband contributions of non-interacting electrons, or whether they involve the interaction-induced incoherent excitations as well, remains to be clarified.

Earlier ARPES measurements in LaOFeP, however, did not see any indication of the incoherent features [42]. This could suggest that the correlation effects are considerably weaker in LaOFeP. Since the Fermi surface appearing in the ARPES measurement [42] is much larger than that appearing in a bulk de Haas - van Alphen (dHvA) experiment [43], an alternative possibility is that due to some surface contamination, the states at the surface that are probed by ARPES are somewhat overdoped [42]. In that case the incoherent features will be significantly suppressed. This possibility could also reconcile the ARPES result with the optical conductivity measurements in LaOFeP, which [44] have shown features similar to those of the parent iron arsenides, namely reduced Drude weight and temperature-induced transfer between low-energy and high energy spectral weights.

In V_2O_3 , again as a comparison, both the coherent and incoherent features have been observed in photoemission experiments [45, 46].

4.2. Fermi surface

The decomposition of the single-electron excitations into coherent and incoherent ones can be realized by a decomposition of the d -electron field operators, thus $d = d^{coh} + d^{incoh}$, with d^{coh} containing a fraction of spectral weight w , and d^{incoh} containing $1-w$. The low-energy single-electron excitations are described in terms of d^{coh} , which can be normalized by w through $c = d^{coh}/\sqrt{w}$ (see below).

The coherent part of the single-electron Green's function is formally derived from the non-interacting Green's function by a self-energy function. Various microscopic approaches – such as DMFT or slave-boson approaches – are able to capture this effect using a momentum (*i.e.* \mathbf{k})–independent self energy, which leads to a Fermi surface that is identical to that of the non-interacting case. Conversely, the consistency of the measured Fermi surface with its non-interacting counterpart (derived from LDA bandstructure calculations, for example) only implies that the self energy is largely \mathbf{k} –independent, and cannot by itself be used to infer the degree of electron correlations.

This last statement also applies to the antiferromagnetically ordered state in the parent iron arsenides. In the incipient Mott picture, even though the driving force for the antiferromagnetism does not come from a Fermi-surface nesting, the antiferromagnetic order parameter will on general grounds (and also through microscopic considerations, Sec. 5) introduce a staggered magnetic field, $\mathbf{h}_{AF}(\mathbf{r}) = \Delta e^{i\mathbf{Q}\cdot\mathbf{r}}$, which will be coupled to the coherent itinerant electrons. This results in a coupling term,

$$\Delta \cdot \sum_{\mathbf{k}} M_{\alpha,\beta} c_{\mathbf{k}+\mathbf{Q}\alpha\sigma}^\dagger \boldsymbol{\tau}_{\sigma,\sigma'} c_{\mathbf{k}\beta\sigma'} \quad (1)$$

where $M_{\alpha,\beta}$ specifies the details of the structure in the orbital space (α, β, \dots), $\boldsymbol{\tau}$ are the Pauli matrices, and repeated symbols are summed. This coupling has the same form

as that in the case of an SDW state and it leads to similar hybridized bands and the opening of the gap centered around the “hot spots” on the Fermi surface (the Fermi momenta \mathbf{k}_F for which $\epsilon_{\mathbf{k}_F} = \epsilon_{\mathbf{k}_F+\mathbf{Q}}$). Precisely this type of band reconstruction has recently been reported in an ARPES experiment [47], which is also largely consistent with the dHvA measurement [48]. Our discussion shows that the reconstruction cannot be used to infer the strength of correlation effects.

We comment on the effective mass of the low-energy excitations; it will be enhanced compared to the LDA bandstructure value. But the effective mass extracted in many measurements – including thermodynamics and single-particle dispersion – will be smaller than $1/w$ because of the non-zero exchange coupling (see the next section). The mass enhancement (measured with respect to the band mass at the Fermi energy) estimated from dHvA [48] is about 2, and that from ARPES ranges from 2-4 and can be orbitally selective [41]. Separately, ARPES measurements have also been used to estimate the band narrowing [defined by the ratio of the LDA-calculated value to the measured value, for the separation between the bottom of the bands containing the electron pockets near the M point $\equiv (\pi, 0)$ and the top of the bands containing the hole pockets near $\Gamma \equiv (0, 0)$] to be about 5 [49, 41].

5. Magnetic order and dynamics

We now derive the low-energy effective Hamiltonian. We can separately consider the on-site Coulomb interactions, including the Hund’s coupling, and the kinetic energy. The interactions at each site can be diagonalized into local configurations, which naturally divide into low energy and high energy sectors. A typical kinetic term of the Hamiltonian has the form of $H_t = \sum t_{ij}^{\alpha\beta} d_{i\alpha\sigma}^\dagger d_{j\beta\sigma}$. With the decomposition $d = d^{coh} + d^{incoh}$, H_t can be rewritten as the sum of three terms:

$$\begin{aligned} H_{t1} &= \sum t_{ij}^{\alpha\beta} d_{i\alpha\sigma}^{\dagger coh} d_{j\beta\sigma}^{coh} \\ H_{t2} &= \sum t_{ij}^{\alpha\beta} d_{i\alpha\sigma}^{\dagger incoh} d_{j\beta\sigma}^{incoh} \\ H_{t3} &= \sum t_{ij}^{\alpha\beta} \left(d_{i\alpha\sigma}^{\dagger coh} d_{j\beta\sigma}^{incoh} + H.c. \right) \end{aligned} \quad (2)$$

We can now discuss the form of the low-energy effective Hamiltonian. $d_{i\beta\sigma}^{coh}$ describes low-energy electronic degrees of freedom, operating entirely within the low-energy sector of the many-body spectra, so H_{t1} is part of the low-energy model. $d_{i\beta\sigma}^{incoh}$, on the other hand, represents high-energy electronic degrees of freedom, connecting the low energy and high energy sectors of the many-body spectra, so we need to project out the high energy sectors in both H_{t2} and H_{t3} .

To do so, we will adopt the projection procedure of Ref. [66]. Here, $d_{\mathbf{k}\alpha\sigma}^{coh}$ appears as the d -electron operator projected to the coherent part of the electronic states near the Fermi energy. (For readers who are inclined to think in terms of the slave-boson-type representation of an electron operator, $d_{\mathbf{k}\alpha\sigma}^{coh}$ corresponds to the part with the slave-boson replaced by its condensate amplitude.) Unlike the full d -electron operator, $d_{\mathbf{k}\alpha\sigma}^{coh}$ does

not satisfy the fermion anticommutation relation: its spectral density integrated over frequency defines w . It will be convenient to introduce $c_{\mathbf{k}\alpha\sigma} = (1/\sqrt{w})d_{\mathbf{k}\alpha\sigma}^{coh}$, which has a total spectral weight normalized to 1 and which satisfies $\{c_{\mathbf{k}\alpha\sigma}, c_{\mathbf{k}\alpha\sigma}^\dagger\} = 1$. We note that $\langle n|d^{coh}|m\rangle$ and $\langle m|d^{\dagger incoh}|n\rangle$ cannot be simultaneously nonzero for any pair of many-body states $|n\rangle$ and $|m\rangle$; in other words, $\langle n|d^{coh}|m\rangle$ is nonzero only when both $|n\rangle$ and $|m\rangle$ belong to the low-energy sector, while $\langle m|d^{\dagger incoh}|n\rangle$ is nonzero only when one of $|n\rangle$ and $|m\rangle$ belongs to the low-energy sector while the other belongs to the high-energy sector. Correspondingly, the single-electron Green's function separates into a coherent part and an incoherent one, and so does the single-electron spectral density. We also note that, in the $w \rightarrow 0$ limit, we reach the Mott transition point where there are only incoherent excitations. For the spectral density of the incoherent excitations at the Mott transition, we will assume [66] (based on the DMFT results [28]) that it is gapped.

To the leading non-vanishing order in w , H_{t2} is then adiabatically connected to the form of the kinetic term deep in the Mott insulating state. The notion of superexchange applies: integrating out the high energy sector of the many-body spectra here will result in a multi-band matrix Heisenberg type of Hamiltonian, H_J . This was done in Ref. [13]. A key feature that differentiates the iron pnictides from other metals lying at the boundary of localization is that H_J must incorporate exchange interactions beyond the nearest-neighbors (n.n.) within the square lattice of the Fe atoms. Indeed, because each As atom has an equal distance from each of the four Fe atoms in a square plaquette, the next-nearest-neighbor interaction, J_2 , is important in addition to the nearest-neighbor interaction, J_1 . This leads to

$$H_J = \sum_{\langle ij \rangle} J_1^{\alpha\beta} \mathbf{s}_{i,\alpha} \cdot \mathbf{s}_{j,\beta} + \sum_{\langle\langle ij \rangle\rangle} J_2^{\alpha\beta} \mathbf{s}_{i,\alpha} \cdot \mathbf{s}_{j,\beta} + \sum_{i,\alpha \neq \beta} J_H^{\alpha\beta} \mathbf{s}_{i,\alpha} \cdot \mathbf{s}_{i,\beta}. \quad (3)$$

where $\langle ij \rangle$ and $\langle\langle ij \rangle\rangle$ label nearest-neighbor (n.n.) and next-nearest-neighbor (n.n.n.) Fe sites on its square lattice. Here, the \mathbf{s} operators are the spins associated with the incoherent part of the electronic excitation; they represent the total electron spin when $w=0$. For convenience, we have also grouped J_H , the on-site Hund's coupling, in H_J . Because of the multiple orbitals, both J_1 and J_2 are matrices. On general grounds [13], the largest eigenvalue of J_2 is expected to be somewhat larger than that of $J_1/2$. Both of these largest eigenvalues are antiferromagnetic in nature.

H_{t1} and H_{t3} can be recast in a convenient form by using $c_{\mathbf{k}\alpha\sigma}$ introduced earlier. After Fourier transform, H_{t1} then becomes

$$H_c = w \sum_{\mathbf{k}, \alpha, \sigma} E_{\mathbf{k}\alpha\sigma} c_{\mathbf{k}\alpha\sigma}^\dagger c_{\mathbf{k}\alpha\sigma} \quad (4)$$

Finally, projecting the high energy sector of the many-body spectra of H_{t3} leads to the following coupling between the local moments and the coherent itinerant carriers:

$$H_m = w \sum_{\mathbf{k}\mathbf{q}\alpha\beta\gamma} G_{\mathbf{k},\mathbf{q}\alpha\beta\gamma} c_{\mathbf{k}+\mathbf{q}\alpha\sigma}^\dagger \frac{\boldsymbol{\tau}_{\sigma\sigma'}}{2} c_{\mathbf{k}\beta\sigma'} \cdot \mathbf{s}_{\mathbf{q}\gamma}, \quad (5)$$

where $\boldsymbol{\tau}$ are the Pauli matrices, and G is generically antiferromagnetic. The final form for the low-energy effective Hamiltonian is

$$H_{eff} = H_J + H_c + H_m. \quad (6)$$

The J_1 - J_2 exchange interactions in the mentioned range lead to a $\mathbf{Q} = (\pi, 0)$ collinear antiferromagnet, which is precisely what has been observed in the parent iron arsenides [50, 51, 52, 53, 54, 55, 56, 57]. Moreover, they cause magnetic frustration which will in turn reduce the ordered moment. (Numerical results on the square-lattice $J_1 - J_2$ model have shown that the frustration-induced suppression of the ordered moment can be substantial [58].) This is also consistent with neutron-scattering observation that the ordered moment in the parent iron arsenides can be as small as $0.3\mu_B/\text{Fe}$ [50, 51, 52, 53, 54, 55, 56, 57], as opposed to the order of $2\mu_B/\text{Fe}$ expected from either ionic considerations or LDA-based *ab initio* calculations.

Another appealing feature that follows from the J_1 - J_2 model is that it leads to an Ising order [15, 16, 59]. The collinear order can be either $\mathbf{Q} = (\pi, 0)$ or $\mathbf{Q}' = (0, \pi)$, with the corresponding magnetic order parameters \mathbf{m} or \mathbf{m}' . The composite scalar, $\mathbf{m} \cdot \mathbf{m}'$, is an Ising order parameter. It is very natural to interpret the structural transition, observed in the parent iron arsenides as originating from a coupling of certain structural degrees of freedom with the Ising order parameter.

The effective Hamiltonian, Eqs. (3,4,5,6), provides the basis to specify the notion of J_1 - J_2 magnetic frustration even though the system is metallic. Note that the J_1 - J_2 couplings have also been studied [60, 61, 62] using *ab initio* calculations. Experimentally, spin waves in the magnetically ordered arsenides are being measured using the inelastic neutron scattering technique [63, 64, 65]. While the results are still preliminary, they have allowed an interpretation based on the J_1 - J_2 model, yielding exchange interactions on the order of 40 meV.

Microscopic studies of the effective Hamiltonian, Eqs. (3,4,5,6), remain to be carried out. This Hamiltonian has the form of a Kondo lattice, in which the Kondo-like coupling of Eq. (5) is in competition with antiferromagnetic exchange interactions among the “local moments” of the incoherent part of the spectrum, Eq. (3). A microscopic analysis should determine w as a function of the bare interactions, and constrain the spectral weight at the Fermi level to be the coherent itinerant carriers; the latter will ensure that the Fermi volume satisfies the Luttinger theorem.

For the purpose of analyzing the magnetic phase diagram of the parent compounds, it would then suffice to use w – as opposed to the bare interactions – as the non-thermal control parameter and to proceed with an effective field theory [14]. A small w does not change the magnetic structure resulting from Eq. (3). Increasing w leads to a magnetic quantum critical point (QCP), to which we now turn.

6. Quantum criticality

For $w = 0$, the magnetic order is captured by the following Ginzburg-Landau action:

$$\begin{aligned} \mathcal{S} = & \int d\mathbf{q} \int d\omega [(r + \omega^2 + c\mathbf{q}^2)((\mathbf{m})^2 + (\mathbf{m}')^2) + v(q_x^2 - q_y^2)\mathbf{m} \cdot \mathbf{m}'] \\ & + \int [u(\mathbf{m})^4 + u(\mathbf{m}')^4 + \tilde{u}(\mathbf{m} \cdot \mathbf{m}')^2 + u'(\mathbf{m})^2(\mathbf{m}')^2] + \dots, \end{aligned} \quad (7)$$

in which $r < 0$ places the system on the magnetically ordered side of the phase diagram. The coupling terms of this quantum sigma model have a similar form as those of their classical counterparts [59].

Non-zero w couples the local moments to the coherent itinerant carriers, as specified by Eq. (5). Its primary effect on the Ginzburg-Landau action is to modify the quadratic coefficient, by introducing a positive shift to r and a damping term. To the leading non-vanishing order in w , the addition to \mathcal{S} is

$$\Delta\mathcal{S} = \int d\mathbf{q} \int d\omega (wA_{\mathbf{Q}} + \gamma|\omega|) [(\mathbf{m})^2 + (\mathbf{m}')^2] \quad (8)$$

The linear-in-frequency damping term, $\gamma|\omega|$, arises because $\mathbf{Q} = (\pi, 0)$ connects the electron and hole pockets of the Fermi surface. This form is valid for $|\omega|$ up to wW , where W is the effective bandwidth of the non-interacting electrons; it is useful to emphasize that the leading term in γ is of the order w^0 , *i.e.* $O(1)$ instead of $O(w)$. Note that, our purpose of considering the Landau damping is primarily to discuss quantum criticality (see below), and we have correspondingly constructed the damping term appropriate for the magnetically disordered case.

The $wA_{\mathbf{Q}}$ term in Eq. (8), where $A_{\mathbf{Q}}$ is a positive constant, is a shift to the mass term of the Ginzburg-Landau theory. Increasing w makes $r(w) = r + wA_{\mathbf{Q}}$ less negative, weakening the magnetic order. This provides a natural account of the neutron-scattering observation [50, 51, 52, 53, 54, 55, 56, 57] that the ordered staggered moment considerably varies across the parent arsenides, ranging from about $0.3\mu_B/\text{Fe}$ to about $0.9\mu_B/\text{Fe}$. This effect is in addition to the variation of the ordered moment due to a change of the J_2/J_1 ratio among the parent arsenides.

Moreover, it is expected that, $r(w_c) = 0$ at a non-zero w_c , which corresponds to an antiferromagnetic quantum critical point (QCP). The linear-in- ω damping implies that the dynamic exponent $z = 2$. One proposal to explore such a magnetic QCP is to use P-substitution for As in the parent arsenides [14]. Experimentally, independent considerations have led to work on the $\text{CeOFeAs}_{1-\delta}\text{P}_{\delta}$ series [67]. It is hoped that it will soon become experimentally feasible to ascertain the degree to which magnetic quantum criticality is realized in the parent iron arsenides.

We note in passing on a particularly intriguing aspect of quantum criticality. Our discussion of the magnetic QCP has focused on the type that conforms to the standard theory based on order-parameter fluctuations. It will be interesting to see whether more unconventional type of quantum criticality, such as those involving a sharp jump of the Fermi surface [77], can come into play in this context.

A magnetic QCP may in principle also occur as a function of carrier doping, which also enhances quantum fluctuations. Carrier doping, however, introduces several features that complicate quantum criticality. First, how carrier doping modifies the Fermi surfaces remains uncertain. In particular, if the magnetic ordering vector \mathbf{Q} no longer connects the electron and hole pockets, the linear-in- ω form of the damping term in Eq. (8) may be absent, and the magnetic QCP will be pre-empted by a QCP associated with the Ising-transition-induced structural distortion [16, 68].

Second, the very fact that carrier doping leads to optimal superconductivity impedes the observation of quantum criticality. Indeed, a variety of behaviors for the zero-temperature phase change from antiferromagnetism to superconductivity [55, 69, 70, 71], have been observed. The complex interplay between magnetic quantum transition and superconductivity is well known, for example in heavy fermion systems, where there are concrete cases – particularly the Rh-based 115 compound – in which a well-defined QCP gets exposed only when superconductivity is suppressed [74, 75, 76, 77]. Unfortunately, the standard means of suppressing superconductivity – applying a magnetic field – is not very easy to implement in the iron pnictides, because the upper critical field H_{c2} appears to be rather high. It is for this reason that focusing on the parent compounds may be more advantageous, where indications are that superconductivity is not as strong as in the doped cases.

Still, there is one particularly appealing feature with the alkali-metal doped 122 system. In $\text{K}_{1-x}\text{Sr}_x\text{Fe}_2\text{As}_2$, the doping x can cover the entire range from 0 to 1 [72]. This opens up a large range of the control parameter space, which is advantageous for identifying the signatures of quantum criticality. Indeed, recent measurements of the electrical and thermoelectric transport properties in this series have provided some support for quantum critical fluctuations in the vicinity of the optimal doping [73].

7. Multiband matrix t - J_1 - J_2 model

From the microscopic point of view, the notion that the parent iron pnictides are in proximity to a Mott insulator provides the basis to consider the doped iron pnictides in terms of a strong coupling approach. The multiband matrix t - J_1 - J_2 model has the form [13]:

$$H_{t-J_1-J_2} = H_t + H_{J_1-J_2},$$

where

$$\begin{aligned} H_t &= \sum_{ij} t_{ij}^{\alpha\beta} \tilde{c}_{i,\alpha}^\dagger \tilde{c}_{j,\beta} \\ H_{J_1-J_2} &= \sum_{\langle ij \rangle} J_1^{\alpha\beta} \mathbf{s}_{i,\alpha} \cdot \mathbf{s}_{j,\beta} + \sum_{\langle\langle ij \rangle\rangle} J_2^{\alpha\beta} \mathbf{s}_{i,\alpha} \cdot \mathbf{s}_{j,\beta} + \sum_{i,\alpha \neq \beta} J_H^{\alpha\beta} \mathbf{s}_{i,\alpha} \cdot \mathbf{s}_{i,\beta}. \end{aligned} \quad (9)$$

Here the multiple bands are labeled by the orbital indices α, β as before and $\tilde{c}_{\alpha,i}$ describe the constrained fermions at the site i . The n.n. and n.n.n. hybridization matrices are

$t_{n.n}^{\alpha\beta} = t_1^{\alpha\beta}$ and $t_{n.n.n} = t_2^{\alpha\beta}$. As noted, the n.n. ($\langle ij \rangle$) and n.n.n. ($\langle\langle ij \rangle\rangle$) superexchange matrices are $J_{n.n}^{\alpha\beta} = J_1^{\alpha\beta}$ and $J_{n.n.n.}^{\alpha\beta} = J_2^{\alpha\beta}$.

This model can be used to study a number of issues that bear on the correlated-electron physics of the carrier-doped iron pnictides. An intriguing possibility is that a carrier-doped state from a parent system with a non-zero but small w behaves similarly to that from a parent system with $w = 0$.

8. Summary

Our discussions above lead to the picture that the iron pnictides have intermediately-strong electron correlations, and are located at the boundary between localization and itinerancy. The proximity to the Mott insulating state separates the single-electron excitations into coherent and incoherent ones, which in turn provide the basis to discuss magnetism and magnetic fluctuations in terms of a combination of local moments and itinerant carriers. Tuning the degree of itinerancy provides a means to vary the strength of magnetic ordering, and leads to a magnetic quantum critical point. Finally, this picture also provides the basis to discuss the carrier-doped iron pnictides in terms of a multiband matrix t - J_1 - J_2 model.

This work has been supported in part by the NSF Grant No. DMR-0706625 and the Robert A. Welch Foundation (Q.S.), the NSF of China and PCSIRT (IRT-0754) of Education Ministry of China (J.D.), and the U.S. Department of Energy (J.-X.Z.).

References

- [1] Kamihara Y, Watanabe T, Hirano H and Hosono H 2008 *J. Am. Chem. Soc.* **130** 3296
- [2] Ren Z A, Lu W, Yang J, Yi W, Shen X L, Li Z C, Che G C, Dong X L, Sun L L, Zhou F and Zhao Z X 2008 *Chin. Phys. Lett.* **25** 2215
- [3] Lebegue S 2007 *Phys. Rev. B* **75** 035110
- [4] Singh D J and Du M-H 2008 *Phys. Rev. Lett.* **100** 237003
- [5] Haule K, Shim J H and Kotliar G 2008 *Phys. Rev. Lett.* **100** 226402
- [6] Cao C, Hirschfeld P J and Cheng H-P 2008 *Phys. Rev. B* **77** 220506(R)
- [7] Kuroki K, Onari S, Arita R, Usui H, Tanaka Y, Kontani H and Aoki H 2008 *Phys. Rev. Lett.* **101** 087004
- [8] Raghu S, Qi X-L, Liu C-X, Scalapino D and Zhang S-C 2008 *Phys. Rev. B* **77** 020503(R)
- [9] Lee P A and Wen X-G *Preprint* arXiv:0804.1739
- [10] Fawcett E 1988 *Rev. Mod. Phys.* **60**, 209
- [11] Fawcett E, Alberts H L, Galkin V Yu, Noakes D R and Yakhmi J V 1994 *Rev. Mod. Phys.* **66** 25
- [12] Imada M, Fujimori A and Tokura Y 1998 *Rev. Mod. Phys.* **70** 1039
- [13] Si Q and Abrahams E 2008 *Phys. Rev. Lett.* **101** 076401
- [14] Dai J, Si Q, Zhu J-X and Abrahams E 2009 *Proc. Natl. Acad. Sci. USA* **106** 4118
- [15] Fang C, Yao H, Tsai W-F, Hu J and Kivelson S A 2008 *Phys. Rev. B* **77** 224509
- [16] Xu C, Mueller M and Sachdev S 2008 *Phys. Rev. B* **78** 020501(R)
- [17] Wu J, Phillips P and Castro Neto A H 2008 *Phys. Rev. Lett.* **101** 126401
- [18] Daghofer M, Moreo A, Riera J A, Arrigoni E, Scalapino D J and Dagotto E 2008 *Phys. Rev. Lett.* **101** 237004
- [19] Seo K, Bernevig B A and Hu J 2008 *Phys. Rev. Lett.* **101** 206404

- [20] Chen W-Q, Yang K-Y, Zhou Y and Zhang F-C *Preprint* arXiv:0808.3234
- [21] Laad M S, Craco L, Leoni S and Rosner H *Preprint* arXiv:0810.1607
- [22] Kou S-P, Li T and Weng Z-Y *Preprint* arXiv:0811.4111
- [23] Hackl A and Vojta M *Preprint* arXiv:0812.3394
- [24] Dong J, Zhang H J, Xu G, Li Z, Li G, Hu W Z, Wu D, Chen G F, Dai X, Luo J L, Fang Z and Wang N L 2008 *Europhys. Lett.* **83** 27006
- [25] McWhan D B, Menth A, Remeika J P, Brinkman W F and Rice T M 1973 *Phys. Rev. B* **7** 1920
- [26] Carter S A, Rosenbaum T F, Honig J M and Spalek J 1991 *Phys. Rev. Lett.* **67** 3440
- [27] Matsuura M, Hiraka H, Yamada K and Endoh Y 2000 *J. Phys. Soc. Jpn.* **69** 1503
- [28] Georges A, Kotliar G, Krauth W and Rozenberg M J 1996 *Rev. Mod. Phys.* **68** 13
- [29] Emery V J and Kivelson S A 1995 *Phys. Rev. Lett.* **74** 3253
- [30] Ni N, Bud'ko S L, Kreyssig A, Nandi S, Rustan G E, Goldman A I, Gupta S, Corbett J D, Kracher A and Canfield P C 2008 *Phys. Rev. B* **78** 014507
- [31] Chen G F, Li Z, Dong J, Li G, Hu W Z, Zhang X D, Song X H, Zheng P, Wang N L and Luo J L 2008 *Phys. Rev. B* **78** 224512
- [32] Boris A V, Kovaleva N N, Seo S S A, Kim J S, Popovich P, Matiks Y, Kremer R K and Keimer B 2009 *Phys. Rev. Lett.* **102** 027001
- [33] Hu W Z, Dong J, Li G, Li Z, Zheng P, Chen G F, Luo J L and Wang N L 2008 *Phys. Rev. Lett.* **101** 257005
- [34] Yang J, Huvonen D, Nagel U, Room T, Ni N, Canfield P C, Bud'ko S L, Carbotte J P and Timusk T *Preprint* arXiv:0807.1040v1
- [35] Yeh A, Soh Y-A, Brooke J, Aeppli G, Rosenbaum T F and Hayden S M 2002 *Nature* **419** 459
- [36] Thomas G A, Rapkine D H, Carter S A, Rosenbaum T F, Metcalf P and Honig D F 1994 *J. Low Temp. Phys.* **95** 33
- [37] Thomas G A, Rapkine D H, Carter S A, Millis A J, Rosenbaum T F, Metcalf P and Honig D F 1994 *Phys. Rev. Lett.* **73** 1529
- [38] Rozenberg M J, Kotliar G, Kajueter H, Thomas G A, Rapkine D H, Metcalf P and Honig D F 1995 *Phys. Rev. Lett.* **75** 105
- [39] Baldassarre L, Perucchi A, Nicoletti D, Toschi A, Sangiovanni G, Held K, Capone M, Ortolani M, Malavasi L, Marsi M, Metcalf P, Postorino P and Lupi S 2008 *Phys. Rev. B* **77** 113107
- [40] Perucchi A, Marini C, Valentini M, Postorino P, Sopracase R, Dore P, Hansmann P, Jepsen O, Sangiovanni G, Toschi A, Held K, Topwal D, Sarma D D and Lupi S *Preprint* arXiv:0811.2154v1
- [41] Ding H, Nakayama K, Richard P, Souma S, Sato T, Takahashi T, Neupane M, Xu Y-M, Pan Z-H, Federov A V, Wang Z, Dai X, Fang Z, Chen G. F., Luo J L and Wang N L *Preprint* arXiv:0812.0534v1
- [42] Lu D H, Yi M, Mo S-K, Erickson A S, Analytis J, Chu J-H, Singh D J, Hussain Z, Geballe T H, Fisher I R and Shen Z-X 2008 *Nature* **455** 81
- [43] Coldea A I, Fletcher J D, Carrington A, Analytis J G, Bangura A F, Chu J-H, Erickson A S, Fisher I R, Hussey N E and McDonald R D 2008 *Phys. Rev. Lett.* **101** 216402
- [44] Qazibash M M, Hamlin J J, Baumbach R E, Maple M B and Basov D N *Preprint* arXiv:0808.3748v1
- [45] Mo S-K, Denlinger J D, Kim H-D, Park J-H, Allen J W, Sekiyama A, Yamasaki A, Kadono K, Suga S, Saitoh Y, Muro T, Metcalf P, Keller G, Held K, Eyert V, Anisimov V I and Vollhardt D 2003 *Phys. Rev. Lett.* **90** 186403
- [46] Mo S-K, Kim H-D, Denlinger J D, Allen J W, Park J-H, Sekiyama A, Yamasaki A, Suga S, Saitoh Y, Muro T and Metcalf P 2006 *Phys. Rev. B* **74** 165101
- [47] Hsieh D, Xia Y, Wray L, Qian D, Gomes K K, Yazdani A, Chen G F, Luo J L, Wang N L and Hasan M Z *Preprint* arXiv:0812.2289v1
- [48] Sebastian S E, Gillett J, Harrison N, Lau P H C, Mielke C H and Lonzarich G G 2008 *J. Phys.: Condens. Matter* **20** 422203
- [49] Yang L X, Zhang Y, Ou H W, Zhao J F, Shen D W, Zhou B, Wei J, Chen F, Xu M, He C, Chen Y, Wang Z D, Wang X F, Wu T, Chen X H, Arita m, Shimada K, Taniguchi M, Lu Z Y, Xiang

- T and Feng D L *Preprint* arXiv:0806.2627v2
- [50] Cruz C de la, Huang Q, Lynn J W, Li J, Ratcliff II W, Zarestky J L, Mook H A, Chen G F, Luo J L, Wang N L and Dai P C 2008 *Nature* **453** 899
- [51] Qiu Y, Bao W, Huang Q, Yildirim T, Simmons J, Lynn J W, Gasparovic Y C, Li J, Green M, Wu T, Wu G and Chen X H 2008 *Phys. Rev. Lett.* **101** 257002
- [52] Chen Y, Lynn J W, Li J, Li G, Chen G F, Luo J L, Wang N L, Dai P C, Cruz C de la and Mook H A 2008 *Phys. Rev. B* **78** 064515
- [53] Kimber S A, Argyriou D N, Yokaichiya F, Habicht K, Gerischer S, Hansen T, Chatterji T, Klingeler R, Hess C, Behr G, Kondrat A and Buechner B *Preprint* arXiv:0807.4441
- [54] Zhao J, Huang Q, Cruz C de la, Lynn J W, Lumsden M D, Ren Z A, Yang J, Shen X L, Dong X L, Zhao Z-X and Dai P C 2008 *Phys. Rev. B* **78** 132504
- [55] Zhao J, Huang Q, Cruz C de la, Li S L, Lynn J W, Chen Y, Green M A, Chen G F, Li G, Li Z, Luo J L, Wang N L and Dai P C 2008 *Nature Materials* **7** 953
- [56] Huang Q, Qiu Y, Bao W, Lynn J W, Green M A, Chen Y, Wu T, Wu G and Chen X H 2008 *Phys. Rev. Lett.* **101** 257003
- [57] Jesche A, Caroca-Canales N, Rosner H, Borrmann H, Ormeci A, Kasinathan D, Kaneko K, Klauss H H, Luetkens H, Khasanov R, Amato A, Hoser A, Krellner C and Geibel C 2008 *Phys. Rev. B* **78** 180504(R)
- [58] Darradi R, Derzhko O, Zinke R, Schulenburg J, Kruger S E and Richter J 2008 *Phys. Rev. B* **78** 214415
- [59] Chandra P, Coleman P and Larkin A I 1990 *Phys. Rev. Lett.* **64** 88
- [60] Yildirim T 2008 *Phys. Rev. Lett.* **101** 057010
- [61] Ma F, Lu Z-Y and Xiang T 2008 *Phys. Rev. B* **78** 224517
- [62] Yin Z P, Lebegue S, Han M J, Neal B P, Savrasov S Y and Pickett W E 2008 *Phys. Rev. Lett.* **101** 047001
- [63] Zhao J, Yao D-X, Li S, Hong T, Chen Y, Chang S, Patchell II W, Lynn J W, Mook H A, Chen G F, Luo J L, Wang N L, Carlson E W, Hu J and Dai P 2008 *Phys. Rev. Lett.* **101** 167203
- [64] Ewings R A, Perring T G, Bewley R I, Guidi T, Pitcher M J, Parker D R, Clarke S J and Boothroyd A T 2008 *Phys. Rev. B* **78** 220501(R)
- [65] McQueeney R J, Diallo S O, Antropov V P, Samolyuk G, Broholm C, Ni N, Nandi S, Yethiraj M, Zarestky J L, Pulikkotil J J, Kreyssig A, Lumsden M D, Harmon B N, Canfield P C and Goldman A I *Preprint* arXiv:0809.1410
- [66] Moeller G, Si Q, Kotliar G, Rozenberg M and Fisher D S 1995 *Phys. Rev. Lett.* **74** 2082
- [67] Geibel C, Krellner C and Jesche A 2008 *private communication*
- [68] Qi Y and Xu C *Preprint* arXiv:0812.0016
- [69] Drew A J, Niedermayer Ch, Baker P J, Pratt F L, Blundell S J, Lancaster T, Liu R H, Wu G, Chen X H, Watanabe I, Malik V K, Dubroka A, Roessle M, Kim K W, Baines C and Bernhard C *Preprint* arXiv:0807.4876
- [70] Luetkens H, Klauss H-H, Kraken M, Litterst F J, Dellmann T, Klingeler R, Hess C, Khasanov R, Amato A, Baines C, Hamann-Borrero J, Leps N, Kondrat A, Behr G, Werner J and Buechner B *Preprint* arXiv:0806.3533
- [71] Chen H, Ren Y, Qiu Y, Bao W, Liu R H, Wu G, Wu T, Xie Y L, Wang X F, Huang Q and Chen X H 2009 *Europhys. Lett.* **85** 17006
- [72] Sasmal K, Lv B, Lorenz B, Guloy A M, Chen F, Xue Y-Y and Chu C W 2008 *Phys. Rev. Lett.* **101** 107007
- [73] Gooch M, Lv B, Lorenz B, Guloy A M and Chu C W *Preprint* arXiv:0812.1927
- [74] Park T, Ronning F, Yuan H Q, Salamon M B, Movshovich R, Sarrao J L and Thompson J D 2006 *Nature* **440** 65
- [75] Knebel G, Aoki D, Braithwaite D, Salce B and Flouquet J 2006 *Phys. Rev. B* **74** 020501
- [76] Knebel G, Aoki D, Brison J-P and Flouquet J *Preprint* arXiv:0808.3687
- [77] Gegenwart P, Si Q and Steglich F 2008 *Nat. Phys.* **4** 186